ANALYSIS OF TOTAL DOSE EFFECTS IN A LOW-DROPOUT VOLTAGE REGULATOR

By

Vishwa Ramachandran

Thesis

Submitted to the Faculty of the

Graduate School of Vanderbilt University

in partial fulfillment of the requirements

for the degree of

MASTER OF SCIENCE

in

Electrical Engineering

December, 2006

Nashville, Tennessee

Approved:

Ronald D. Schrimpf

Daniel M. Fleetwood

ACKNOWLEDGMENT

It is said that attitude and not aptitude, determines ones altitude. In research, a person can reach higher altitudes only by determination and perseverance. These are qualities which need to be sustained over the period of research, and I find that I have the satisfaction of having achieved this in my research, thanks to people around me.

My Adviser, Professor Ron Schrimpf, has been a constant source of inspiration, knowledge, wisdom and encouragement with his friendly but resilient approach; something I can identify myself with. Through this work, I have come to being associated with Professor Dan Fleetwood along with Professor Schrimpf. I can only say that I have been very lucky in having an opportunity to work with two among the best in research. They have persevered and stood by me when the going was tough and I am grateful towards them for that. I have also benefited from many a fruitful discussion with Professor Art Witulski from ISDE. His disarming nature and thoughtful insights have helped me immensely in understanding how a complex problem can be looked upon as a set of simple ones. I have also taken advantage of Professor Tim Holman's ready-to-fix solutions to the problems that I have posed to him and thank him for his support. Professor High Barnaby of Arizona State University deserves a special mention for giving helpful pointers at a critical stage in the Thesis work. Thanks also to Dr. Anthony Hmelo, Aditya Karmarkar and Aditya Kalavagunta in helping me out with the characterization work at Vanderbilt University. Professor Vivek Agarwal of the Department of Electrical Engineering at the Indian Institute of Technology, Bombay, deserves a special mention for moulding and guiding me into

the field of research in Electrical Engineering. I have learned a lot under his dedicated and focused direction.

In a research environment, friends at work become an integral part of one's life and I have a great time with each and everyone's company here at RER. I enjoy both working and hanging out with them. It just adds variety into this academic life, which can turn out to be monotonous at times. Other people who have helped me maintain this balance between academics and life outside it include my roommates, both past and present, my li'l brother Montel and my time with him and his family, people from Big Brothers and Big Sisters of Middle Tennessee and the Champ athletes I have come across. They are all my inspiration as well as best friends.

Last but not by any long shot, the least, I owe so much to my parents and my brother and sister. They have been with me through thick and thin, and always so understanding and encouraging, never making me feel that they are so far away from me. I am truly grateful towards them. To my dad, who retired at the end of last year, I dedicate this Thesis to him.

TABLE OF CONTENTS

Page

ACKNOWLEDGMENT ii

LIST OF FIGURES vi

Chapter

I. INTRODUCTION 1

Historical Perspective 1
The Low-Dropout Voltage Regulator 2
Motivation and Scope of Work 4

II. OVERVIEW OF RADIATION EFFECTS ON BIPOLAR DEVICES . 5

Gain Degradation in Bipolar Devices 5
Enhanced Low Dose Rate Sensitivity 6
Other Radiation-induced Effects 7

III. EXPERIMENTS AND CIRCUIT EXTRACTION 9

Total Dose Experiments 9
Electrical Characterization 10
Circuit Extraction 10

IV. CIRCUIT ANALYSIS 13

Modeling Preirradiation Characteristics 13
Operation of Critical Transistor Blocks 14

V. EXPERIMENTAL RESULTS 17

Response at Low Dose Rate 17
Response at Elevated Temperature Irradiation 19
Response at High Dose Rate Irradiation 22

VI. ANALYSIS OF THE RADIATION RESPONSE 24

Gain Degradation 24
Collector-Emitter Leakage 26
Summary of Modeling Parametric Variations 31

VII. ANNEALING MECHANISMS 34

Annealing after High Dose Rate Irradiation 34
Annealing after Elevated Temperature Irradiation 37

VIII. CONCLUSIONS 38

REFERENCES 40

LIST OF FIGURES

Figure Page

1. LDO voltage regulator block schematic diagram 3

2. Normalized current gain as a function of base-emitter voltage in an NPN BJT, for different total ionizing doses. 5

3. Normal current gain vs. dose rate for a lateral PNP BJT irradiated to a total dose of 20 krad(Si) as a function of dose rate. (After [29]). 7

4. (a) Die-photo of the MIC29372 LDO voltage regulator (b) Extracted circuit schematic diagram of the MIC29372 LDO voltage regulator. . . 11

5. Preirradiation load regulation characteristics of the LDO. 13

6. Preirradiation and postirradiation experimental line regulation characteristics at low dose rate, when the LDO voltage regulator is biased without load during irradiation. 18

7. Preirradiation and postirradiation experimental load regulation characteristics at low dose rate, when the LDO voltage regulator is biased without load during irradiation. Postirradiation output voltages beyond I_{load} of 300 mA are not plotted. 19

8. Preirradiation and postirradiation experimental line regulation characteristics at elevated temperature, when the LDO voltage regulator is biased without load during irradiation. 20

9. Preirradiation and postirradiation experimental load regulation characteristics at elevated temperature, when the LDO voltage regulator is biased without load. Postirradiation output voltages beyond I_{load} of 300 mA are not plotted. 21

10. Preirradiation and postirradiation experimental output line regulation characteristics at high dose rate, when the LDO is biased without load during irradiation. 22

11. Preirradiation and postirradiation experimental output load regulation characteristics at high dose rate, when the LDO voltage regulator is biased without load during irradiation. Postirradiation output voltages beyond I_{load} of 580 mA are not plotted. 23

12. Pre- and post-irradiation offset voltages of the op-amp block show how the droop in the postirradiation output voltage can be modeled as gain degradation in the differential amplifiers and the output pass transistor. 25

13. Modeling of C-E leakage by inserting a high-resistance between collector and emitter terminals of Q_1. 28

14. Simulation results showing the influence of pass transistor degradation on the load regulation response of the LDO in the case where the LDO is biased and loaded during irradiation. Output voltages that go below 4.5 V for higher load currents are not plotted. 29

15. Pre- and post-irradiation and post-anneal characterization of the 10× bandgap transistor Q_1. 31

16. Modeled changes in I_{se} for all three dose rates and corresponding bias conditions. The dashed lines represent modeling for NPNs while the solid lines represent the modeling done for PNPs. 32

17. Modeled changes in β_F for all three dose rates and corresponding bias conditions. The dashed lines represent modeling for NPNs while the solid lines represent the modeling done for PNPs. 33

18. Modeled changes in N_e for all three dose rates and corresponding bias conditions. The dashed lines represent modeling for NPNs while the solid lines represent the modeling done for PNPs. 33

19. Experimental postirradiation anneal for high dose rate, bias with load, load regulation characteristics. The second anneal curve is not plotted since it overlaps the first one. 34

20. Experimental postirradiation anneal for high dose rate, grounded load regulation characteristics. The second anneal curve is not plotted since it overlaps the first one. 35

21. Experimental postirradiation anneal for elevated temperature irradiation, bias without load, load regulation characteristics. The second anneal curve is not plotted since it overlaps the first one. 36

CHAPTER I

INTRODUCTION

Historical Perspective

The invention of the p-n junction transistor [1] ushered in a new era in the history of semiconductors. As solid-state semiconductor devices came into use in space and military applications, research into the effects of space and nuclear radiation on these devices gained importance. Since discrete bipolar devices were the order of the day, the focus of radiation effects research was initially concerned with displacement damage from neutrons and protons on bipolar devices [2]. The failure of the communications satellite Telstar in 1962 [3] shifted focus towards understanding failure of bipolar devices on account of total ionizing dose [4]. Starting from discrete transistors in the 60s, the past three decades have seen research into the effects of total ionizing dose on linear and I^2L bipolar circuits, recessed field oxide digital circuits and most recently, the low dose rate sensitivity of bipolar linear circuits [5].

In accordance with Moore's law, which states that the number of transistors on a chip would double every two years, modern microcircuits have been pushing the limits as far as device feature sizes and packing densities are concerned. Most of the changes have been effected on CMOS devices as compared to bipolar technologies. However, space system designs always have been conservative, lagging several generations behind the current state-of-art. This is not very surprising, since today's advanced microcircuits are far more susceptible to transient, high-energy particle hits (i.e. single event effects) and many effects are not completely understood, however

impressive their ground-based performance might be. Thus, space systems still use a lot of older, bipolar technologies that have advantages over their CMOS counterparts in the area of speed [6], transconductance [7], linearity and current drive. Also, many of the radiation-induced failure mechanisms in linear microcircuits using older bipolar technologies are understood to a large extent, thanks to extensive research carried out on them.

The Low-Dropout Voltage Regulator

One important member of the linear bipolar family is the voltage regulator. A linear regulator provides a stable, DC voltage under varying loads within specifications and thus is an integral part of any electronic system. In particular, low-dropout (LDO) voltage regulators have been the subject of radiation-effects investigation [8]-[13].

A LDO voltage regulator supplies a desired load current at lower dropout voltages compared to standard linear regulators. Dropout voltage is defined as the minimum input-output voltage differential required to maintain normal regulator operation. LDO voltage regulators use an output pass transistor (PNP or NPN) between their input and output terminals, as shown in Fig. 1.

The main circuit blocks of a LDO voltage regulator include the bandgap reference circuitry, the operational amplifier (op amp) circuitry and the output pass transistor. The bandgap voltage circuitry generates a temperature-independent bandgap voltage within operational limits. The operational amplifier (op amp) is a differential transistor pair that acts as an error amplifier. Its role in the circuit is to maintain equal voltages at its input terminals. The reference voltage V_{BG} is fed to one of the

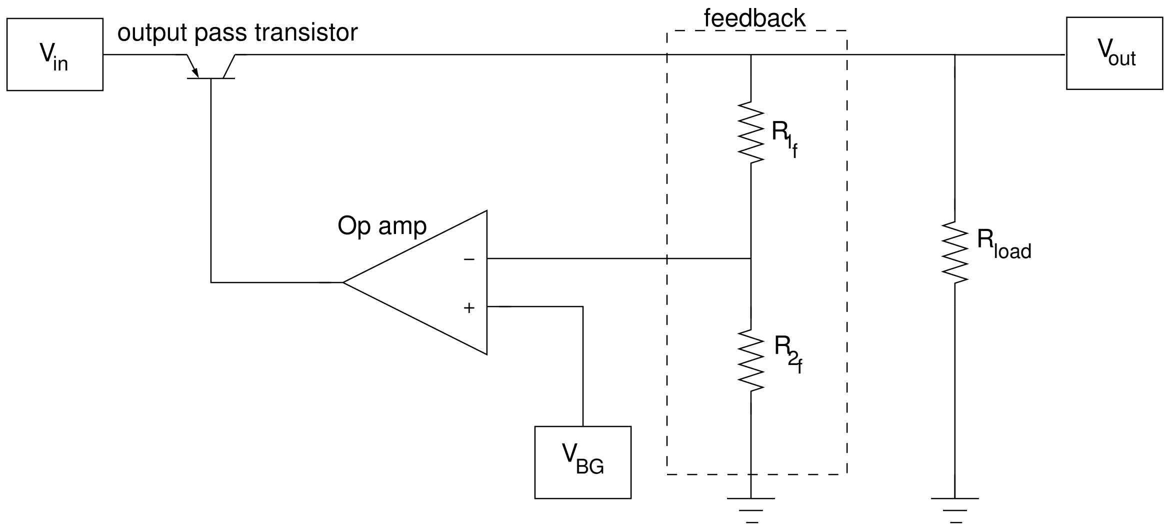

Figure 1: LDO voltage regulator block schematic diagram

input terminals of the op amp, while the other input is the feedback voltage through resistors R_{1_f} and R_{2_f}. The op amp maintains tight feedback in the circuit by keeping its offset voltage as low as possible.

The output pass transistor conducts most of the load current, and hence dissipates most of the power in a LDO voltage regulator. On account of this, the output pass transistor is usually the largest transistor in a LDO voltage regulator, in terms of size. The magnitude of the collector-to-emitter voltage V_{CE} of the pass transistor determines the dropout voltage of the LDO voltage regulator. Since this value is typically less than or equal to 0.2 V, LDO voltage regulators dissipate low power and dominate battery-powered applications, especially in space. In Fig. 1, R_{load} represents the external load resistance for the load current. This may be either an active (current source) or a passive (resistive) load. The output voltage V_{out} of a LDO voltage regulator is given by:

$$V_{out} = \left(1 + \frac{R_1}{R_2}\right) \times V_{BG} \quad (1)$$

Motivation and Scope of Work

Several types of LDO voltage regulators have been shown to exhibit enhanced low-dose-rate sensitivity (ELDRS) [10, 11], and complex circuit responses to total ionizing dose. For example, while operational amplifiers and comparators typically become worse after annealing due to gain degradation associated with increasing interface-trap formation after radiation exposure, some LDO voltage regulators instead recover during annealing [14]. These issues prompted a detailed evaluation of total dose effects for LDO voltage regulators from a circuit-level perspective.

In this thesis, the circuit elements responsible for the irradiation and annealing response of a positive LDO voltage regulator, the MIC29372 from Micrel, are identified. With the aid of circuit-level simulations and experimental data, key circuit elements that bound the post-irradiation and post-anneal response are identified and their degradation mechanisms explained. Chapter II gives an overview of radiation effects research on bipolar devices. Chapters III and IV describe the irradiation experiments carried out on the LDO voltage regulator and the methodology of its circuit extraction and analysis respectively. While Chapter V elaborates on the results of the irradiation experiments at different dose rates, Chapter VI presents corresponding analyses associated with the observed post-irradiation behavior of the LDO voltage regulator. Chapter VII discusses the annealing mechanisms observed in the parts irradiated at high dose rate and at elevated temperature irradiation. Finally, Chapter VIII provides a summary and conclusions of the work.

CHAPTER II

OVERVIEW OF RADIATION EFFECTS ON BIPOLAR DEVICES

Gain Degradation in Bipolar Devices

Gain degradation in bipolar devices has been researched since the 1960s as discussed in Chapter I. The Messenger-Spratt equation [2, 15, 16] described the effects of neutron radiation on bipolar devices, while a similar relationship was developed to explain displacement damage effects [17]. In the case of total ionizing dose, gain degradation depends on the radiation induced-charges generated in the oxide and the recombination centers at the Si/SiO_2 interface [18]-[24].

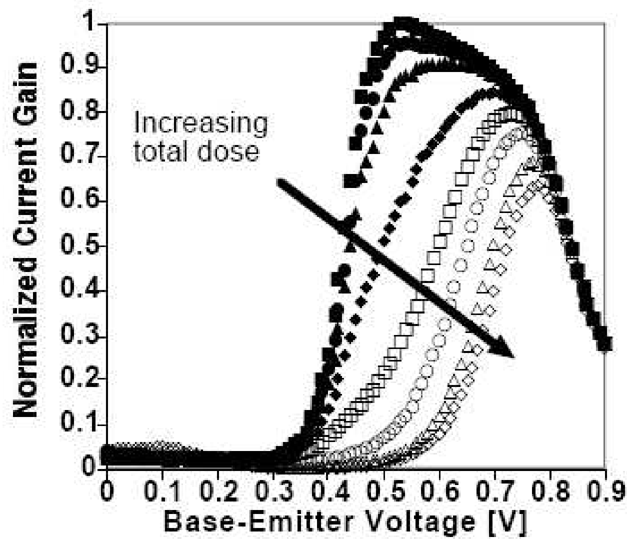

Figure 2: Normalized current gain as a function of base-emitter voltage in an NPN BJT, for different total ionizing doses.

Fig. 2 gives a good idea of how current gain in an NPN BJT changes due to

different total ionizing doses, depending on the value of the base-emitter bias. Significant degradation is seen at lower base-emitter biases and higher total doses in the peak of the current gain. In addition, there are also gain degradaion effects due to protons [25, 26] and heavy-ions [27] that interact in a complex fashion with the effects produced by gamma rays.

Enhanced Low Dose Rate Sensitivity

The first observed ELDRS effect was in 1991 [28], when it was found that the some bipolar devices showed greater gain degradation when they were irradiated at lower dose rates than at higher dose rates, for the same total dose. Moreover, the degradation at low dose rate could not be predicted from high-rate irradiation and post-irradiation annealing. Though dose rates experienced in space fall into the category of low to very low dose rates, ground testing on the devices is usually carried out at much higher dose rates. Thus, this discovery also suggested that the total-dose that can be tolerated in space might be overestimated by conventional test methods [29]. Fig. 3 illustrates the ELDRS effect clearly. The results were found to be a "true dose rate effect" (as opposed to a "time dependent effect") [8, 12, 30].

Models have been developed to explain the phenomenon of ELDRS. The first model, called the "space charge model" explained ELDRS as occurring due to slowly transporting holes at low dose rates [31]-[33]. At higher dose rates, the existing space charge retards transport of holes and protons towards the interface and increases electron-hole recombination, thus reducing the amount of radiation damage. This model was also extended to include electron trapping at high dose rate [34] and reduced interface trap buildup [35]. Another model suggested that the ELDRS effect

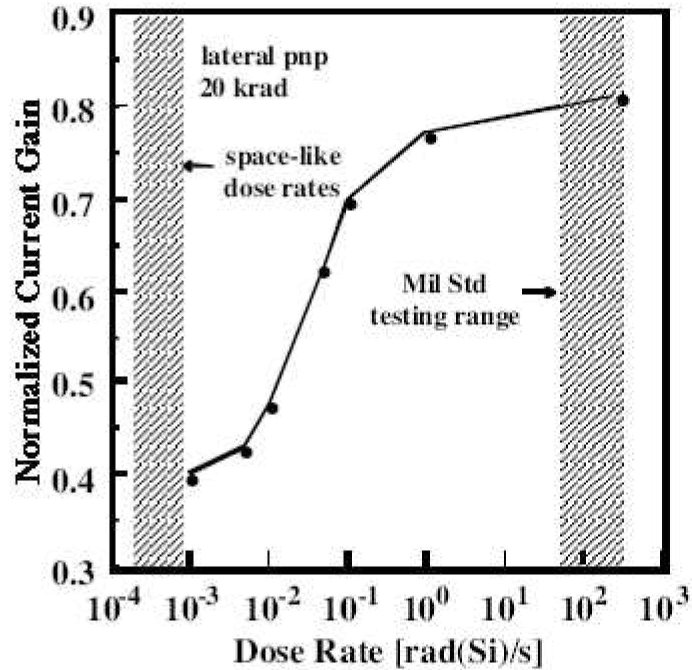

Figure 3: Normal current gain vs. dose rate for a lateral PNP BJT irradiated to a total dose of 20 krad(Si) as a function of dose rate. (After [29]).

may be a delayed reaction rate effect [36, 37] of two species, with different times required for the two species to reach the Si/SiO_2 interface. A third model [38] attributes ELDRS to shallow electron traps in the oxide. At low dose rates, the occupancy of these traps is smaller because of shorter emission times from these shallow traps [39].

Other Radiation-induced Effects

In addition to gain degradation and displacement damage, bipolar devices may also experience radiation-induced leakage current effects. This could be between two bipolar devices or between the collector and emitter of the same device [40]-[44]. In particular, the collector-to-emitter (C-E) leakage has been shown to have effects even at the circuit level [9, 45]. In these papers, a C-E leakage in (the larger of

two transistors of) a Brokaw bandgap circuit was shown to increase the output of a voltage regulator to a total dose of about 200 krad(SiO_2). The C-E leakage caused the bandgap voltage to increase on account of decreased collector current in the larger bandgap transistor, due to which the output increased. Chapter V describes the analysis procedure used to identify this effect in greater detail.

CHAPTER III

EXPERIMENTS AND CIRCUIT EXTRACTION

Total Dose Experiments

Ground-based total-dose experiments were performed in support of the NASA LWS (Living With a Star) SET (Space Environments Testbed) project [46]. One of the aims of the LWS Space Environments Testbed project is to analyze and model radiation-induced performance degradation of components used in spacecraft. The pre- and postirradiation data obtained from the ground-based experiments were used as calibration points for circuit simulations that have been performed to facilitate an understanding of the circuit response. Three types of irradiation experiments on LDO voltage regulators were carried out as part of this project. Low dose rate experiments were done at 10 mrad(SiO_2)/s to a total dose of 50 krad(SiO_2) at room temperature (RT) in a Co-60 room source. High dose rate experiments were carried out at 100 rad(SiO_2)/s to 100 krad(SiO_2) at RT, while elevated temperature irradiation (ETI) experiments were performed at 100°C and 5 rad(SiO_2)/s to 50 krad(SiO_2). The high dose rate and ETI tests were performed in Nordion Gammacell 220 and Shepherd 484 irradiators, respectively.

Samples were irradiated for each of the four bias conditions mentioned above, for each type of exposure. Annealing measurements were made after 16 and 74 days of RT annealing after the high dose rate irradiations. The same procedures were carried out after 14 and 35 days for the ETI parts, which were annealed at 100°C. In all of

the annealing experiments, the devices were biased under the same conditions used during the irradiation experiments.

Electrical Characterization

The MIC29372 is a positive LDO voltage regulator with an output voltage that is programmable from +5 to +26 V, with an option to disable the output by providing an external input, called the "shutdown" input [47]. Electrical characterization during the ground-based tests included conventional line and load regulation analyses before and after radiation exposure, and through postirradiation anneal. Line regulation was determined by measuring V_{out} at different values of input voltage V_{in}, at a constant load current $I_{load} = 100$mA, while load regulation was determined by measuring V_{out} at different I_{load} values, at a constant $V_{in} = +15$ V. All of the electrical measurements used a pulsed current of 5 ms duration for I_{load} at the output, from a minimum value of 5 mA to the maximum value of the desired I_{load}. The nominal V_{out} used for all measurements was +5 V. All of the above tests were carried out at the irradiation and testing facility at NAVSEA Crane.

Circuit Extraction

Based on a die photomicrograph of the MIC29372, the detailed circuit schematic was extracted, as shown in Fig. 4. In particular, three main circuit blocks are important in understanding the radiation response and postirradiation behavior of the LDO voltage regulator. The first block consists of Brokaw bandgap transistors Q_1 and Q_2, with Q_1 having an emitter area 10 times that of transistor Q_2. The other two blocks are the operational amplifier, including the differential transistor pair, Q_{16}

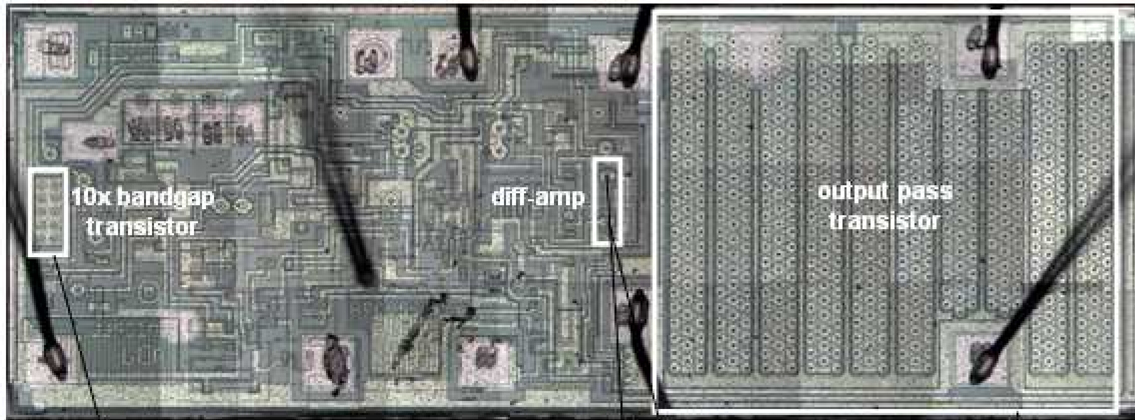

(a)

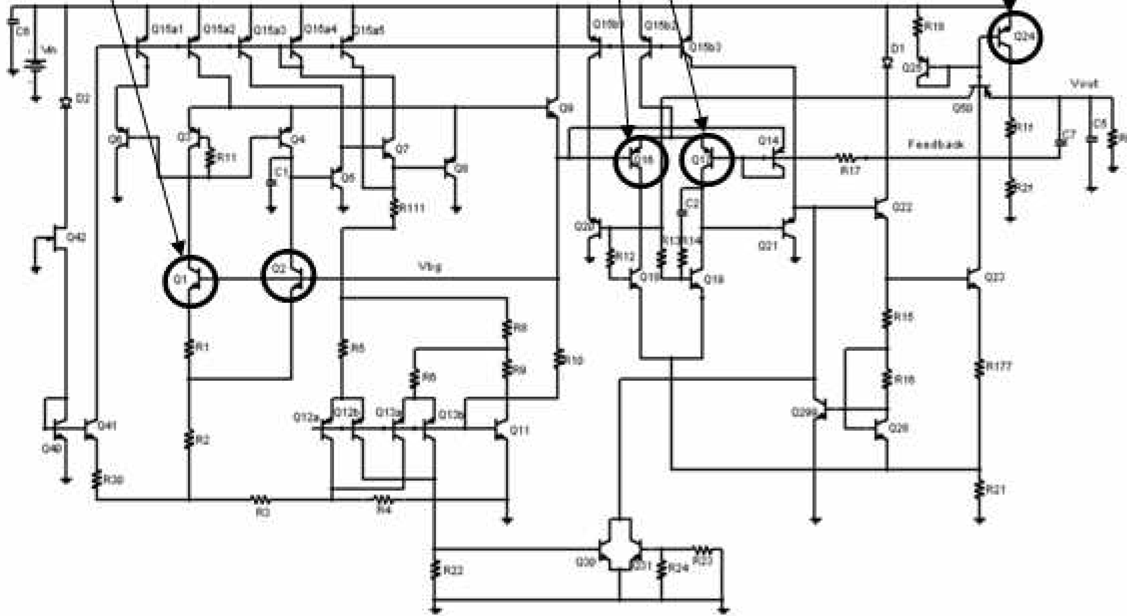

(b)

Figure 4: (a) Die-photo of the MIC29372 LDO voltage regulator (b) Extracted circuit schematic diagram of the MIC29372 LDO voltage regulator.

and Q_{17}, and the output pass transistor Q_{24} that occupies about 40% of the LDO voltage regulator die.

Simulations were performed with device dimensions (perimeters for LPNP transistors and areas for NPN transistors) extracted from the die photos. The forward current gain β_F, the forward base-emitter recombination current I_{se}, and the forward base-current ideality actor N_e were varied in PSPICE models to describe the radiation-induced degradation over a sufficient range to verify that the estimates used, on the basis of previous knowledge of similar circuits built in this technology, were sufficient to describe the circuit response. Pre- and postirradiation models were obtained for the different bias conditions mentioned above.

CHAPTER IV

CIRCUIT ANALYSIS

Modeling Preirradiation Characteristics

A slight droop in V_{out} with increasing I_{load} is typically seen in voltage regulators. However, as shown in Fig. 5, in the preirradiation load regulation experiments performed here, V_{out} increased with increasing I_{load} at currents above 400 mA.

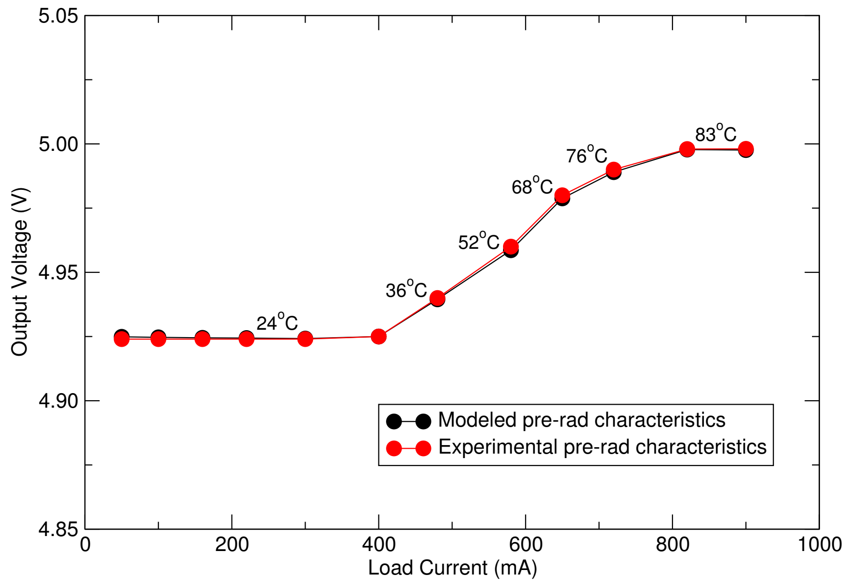

Figure 5: Preirradiation load regulation characteristics of the LDO.

This phenomenon is typically associated with increased die temperature due to the high load current. In an effort to quantify this effect, load regulation data were obtained using an active (pulsed current) source and compared to the results obtained using a passive (load resistor) source. The pulsed current source has an on-time of

5 ms during which power is dissipated, while the resistive load dissipates power on a continuous basis. There was negligible difference in the results obtained using the different current sources, owing to appropriate heat-sinking measures incorporated in the circuit set-up. However, these measures are not able to prevent local heating due to the instantaneous high currents that flow in the circuit. Compared to the output pass transistor, which conducts most of the load current, the other transistors in the circuit conduct much smaller amounts of current. Hence, it was concluded that the increase in V_{out} was primarily due to heating of the output pass transistor at higher I_{load}. Since PSPICE does not allow one to increase the operating temperature of individual transistors, the global temperature settings were varied at every I_{load} above 400 mA to model the experimental data, as shown in Fig. 5. This procedure was found to be satisfactory for the purposes of calibrating the circuit models and using them to help understand the observed results.

Operation of Critical Transistor Blocks

1. **Bandgap circuit:** The Brokaw bandgap circuit in the LDO voltage regulator sets up the V_{BG} as well as V_{out}, as seen from equation (1). The collector currents of transistors Q_1 and Q_2 can be written as:

$$I_{C_1} = I_{S_1} \times \, exp\left(\frac{V_{BE_1}}{V_T}\right) \tag{2}$$

$$I_{C_2} = I_{S_2} \times \, exp\left(\frac{V_{BE_2}}{V_T}\right) \tag{3}$$

Here, I_{S_1} and I_{S_2} are the saturation currents of Q_1 and Q_2, respectively. Since

the emitter of Q_1 is 10 times larger than that of Q_2, it follows that I_{S_1} is 10 times larger than I_{S_2} in magnitude, while Q_2 has a higher V_{BE} than Q_1. Dividing (3) by (2) and rearranging, we get

$$V_{BE_2} - V_{BE_1} = \Delta V_{BE} = V_T \times 10 \times ln\left(\frac{I_{C_2}}{I_{C_1}}\right) \tag{4}$$

where V_T is the thermal voltage. The bandgap voltage V_{BG} is the sum of (4) above and a voltage corresponding to the voltage division in resistors R_{1_f} and R_{2_f} respectively. Thus, any change in the collector currents of either transistor could change ΔV_{BE} (for a given V_{BE} of Q_1 and Q_2), which in turn could change V_{BG} and hence, V_{out} as seen from (1).

2. **Op-amp circuit:** As shown in Fig. 1, the operational amplifier circuit is designed to maintain equal voltages at its input terminals. This means that V_{offset} is of the order of a few mV in practical cases, assuming minimal input bias currents. Since this circuit is made up of a pair of identical PNP BJTs connected as differential transistors, their base currents correspond to the bias currents of the operational amplifier. As the base currents of the transistors increase due to gain degradation during irradiation, the bias currents of the operational amplifier, and hence V_{offset}, also increase. Thus, the operational amplifier is no longer able to maintain tight feedback, and its performance can deteriorate significantly, depending upon the amount of gain degradation in the transistors. Also, since one of its inputs is V_{BG}, deterioration in the bandgap circuitry affects its performance.

3. **Output pass transistor:** The output LPNP pass transistor in the Micrel

LDO has about 650 emitters connected in parallel. Previous work [48, 49] has shown that LPNP transistors in particular, are typically more vulnerable to TID than vertical or substrate PNP transistors, both at low and high dose rates. It has also been shown that the output pass transistor is the main cause of loss of output current drive in the Micrel LDO [11]. Since I_{load} at the output of the LDO voltage regulator is almost equal to the collector current of this pass transistor, radiation-induced gain degradation (and the corresponding increase in base current) affects I_{load} and the corresponding load regulation response of the LDO.

CHAPTER V

EXPERIMENTAL RESULTS

The ground-based NASA-LWS SET experiments were carried out at three different dose rates with four bias conditions at each dose rate. These bias conditions were: bias with load, bias without load, all pins grounded, and the "shutdown" mode of operation. Some of the most significant issues from these experiments are the main points of focus of this thesis. Unless stated otherwise, all results are for irradiations in which the circuit is biased without a load. Results for other irradiation bias conditions are discussed elsewhere [14].

Response at Low Dose Rate

Figure 6 shows the low dose rate (LDR) line regulation response for the "bias without load" case for a dose of 50 krad(SiO_2). Considering only the postirradiation V_{out} curve, it is seen that there is a degradation of regulation (slope change) in V_{out} over the entire range of V_{in}. In addition, the postirradiation V_{out} values are lower than corresponding preirradiation values over the entire range of V_{in}, and the difference between them is much more than that allowed by the manufacturer line regulation specifications [47]. Of the four bias conditions at low dose rate irradiated to the same dose of 50 krad(SiO_2), the "grounded" case showed the largest degradation in both postirradiation V_{out} and regulation.

The low dose rate load regulation for the "bias without load" case for a dose of 50 krad(SiO_2) is shown in Fig. 7.

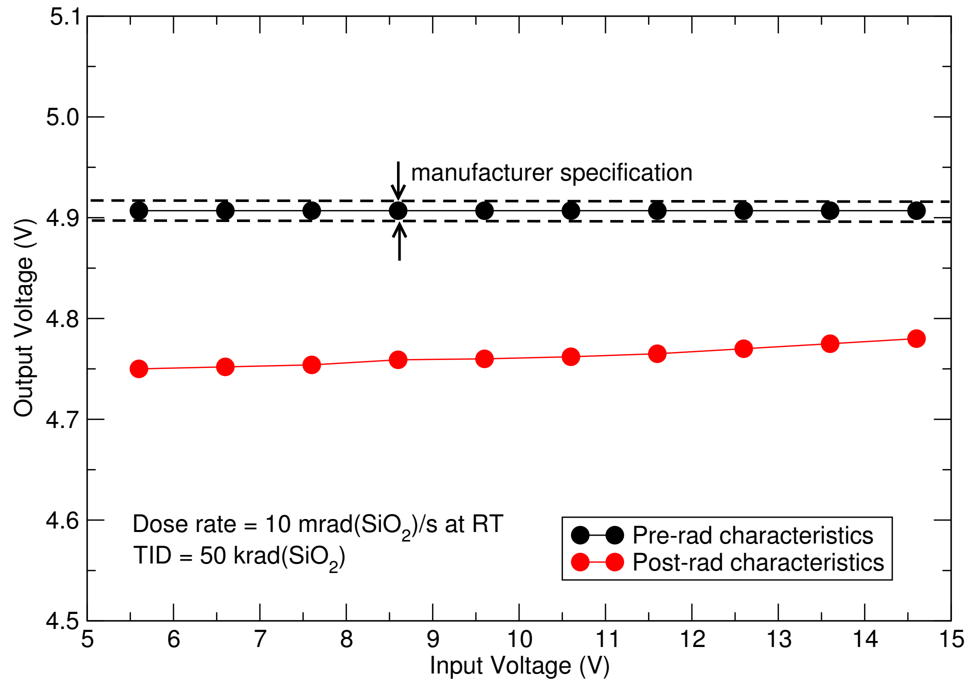

Figure 6: Preirradiation and postirradiation experimental line regulation characteristics at low dose rate, when the LDO voltage regulator is biased without load during irradiation.

In this case too, the postirradiation V_{out} values are lower than corresponding preirradiation values. Also, the LDO voltage regulator shows functional failure for postirradiation V_{out} above 300 mA of I_{load}. The V_{out} trends in load regulation were similar for all bias conditions for parts irradiated to 50 krad(SiO_2) at low dose rates, with the worst-case degradation occurring for the "grounded" case, where the LDO voltage regulator stopped regulating above $I_{load} = 150$ mA at 40 krad(SiO_2). Thus, in the "grounded" case in load regulation, the LDO voltage regulator failed functionally as well as parametrically after 50 krad(SiO_2) at low dose rate.

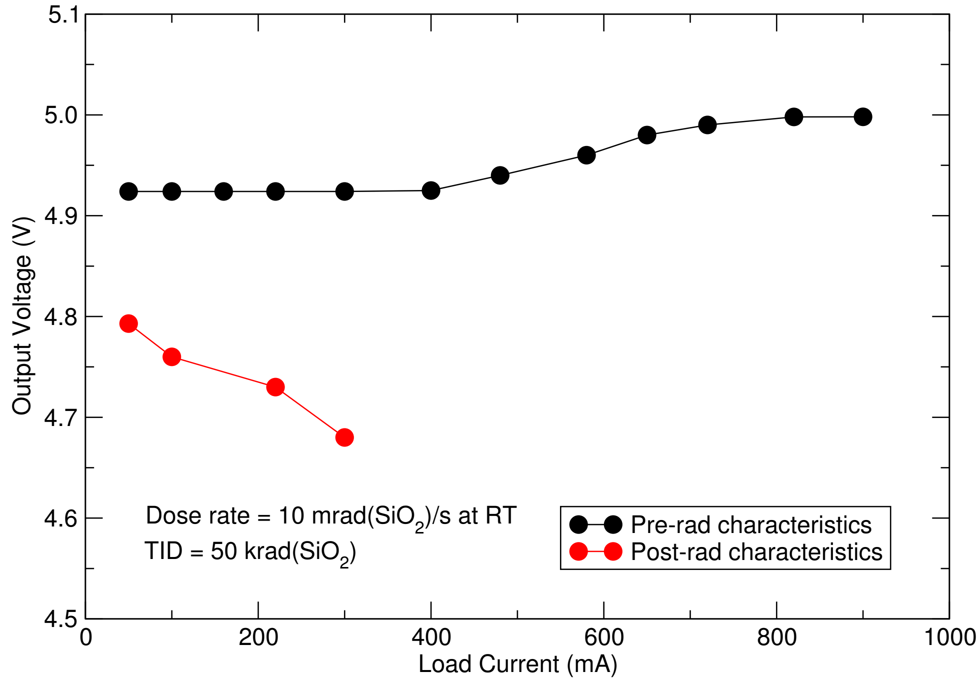

Figure 7: Preirradiation and postirradiation experimental load regulation characteristics at low dose rate, when the LDO voltage regulator is biased without load during irradiation. Postirradiation output voltages beyond I_{load} of 300 mA are not plotted.

Response at Elevated Temperature Irradiation

Figure 8 shows the pre- and postirradiation line regulation characteristics for parts irradiated at elevated temperature to 50 krad(SiO_2) for the "bias without load" condition.

Similar to the low dose rate line regulation trends above, the postirradiation V_{out} exhibits degradation in regulation (slope change) over the entire range of V_{in}. Here too, the postirradiation values of V_{out} are lower than corresponding preirradiation values over the entire range of V_{in}, with the difference greater than manufacturer line regulation specifications [47]. Another similarity was that the "grounded" bias

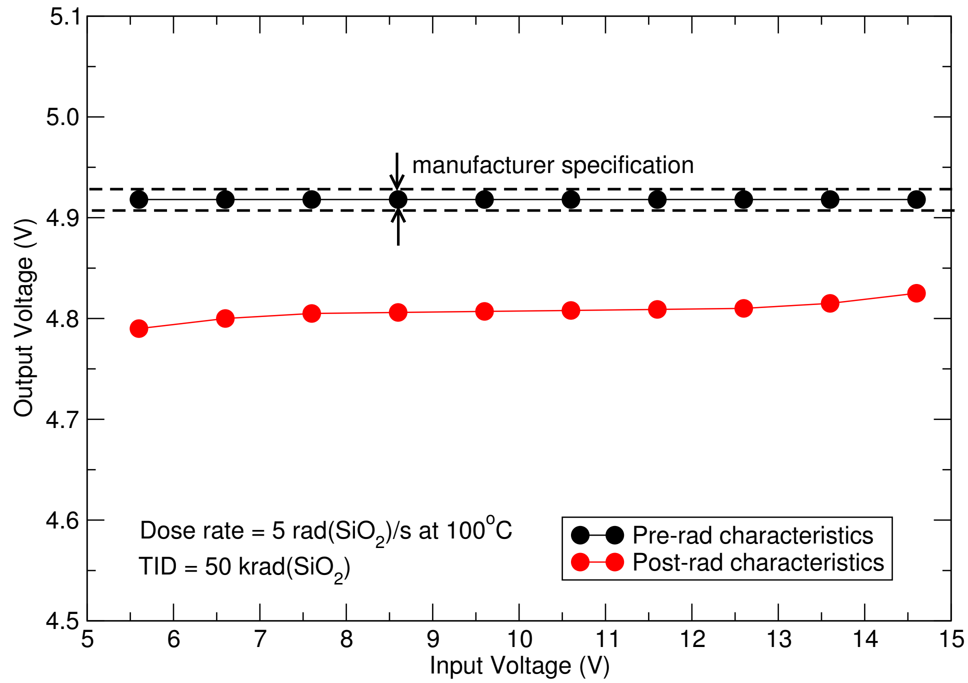

Figure 8: Preirradiation and postirradiation experimental line regulation characteristics at elevated temperature, when the LDO voltage regulator is biased without load during irradiation.

case showed the worst V_{out} and regulation degradation of all four irradiation bias conditions at elevated temperature for a dose of 50 krad(SiO_2).

The difference between pre- and postirradiation V_{out} line regulation values is smaller than that observed in the low dose rate case for the same "bias without load" bias condition and dose. This is also true when one compares the difference in pre- and post-irradiation line regulation V_{out} values for all other bias conditions for irradiation to 50 krad(SiO_2). While there was both degradation of regulation as well as functional failure (at high I_{load}) in the LDO voltage regulator after an ETI exposure to 50 krad(SiO_2), the degradation was lower when compared to that at low dose rate for the same total dose.

Figure 9 shows the pre- and postirradiation V_{out} load regulation trends for the

same bias condition. Again, the postirradiation V_{out} trend observed is similar to that observed in the corresponding low dose rate case. The postirradiation V_{out} values are lower than corresponding preirradiation values and the LDO voltage regulator functionally failed above an I_{load} of 300 mA. Similar V_{out} trends are observed in line and load regulation for the other three bias conditions.

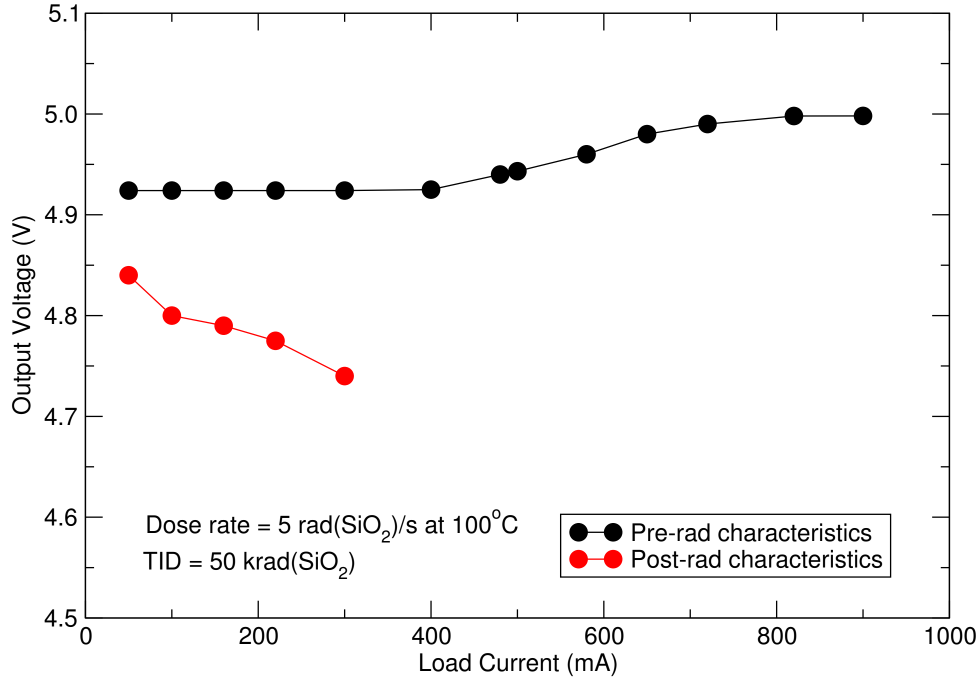

Figure 9: Preirradiation and postirradiation experimental load regulation characteristics at elevated temperature, when the LDO voltage regulator is biased without load. Postirradiation output voltages beyond I_{load} of 300 mA are not plotted.

Annealing at 100°C showed almost complete recovery of line regulation to preirradiation characteristics for all bias conditions. In load regulation, there was complete recovery towards preirradiation characteristics at lower values of I_{load}, but at higher I_{load} values, the recovery was not complete, for all bias conditions, but was within 2% of corresponding preirradiation values. In both cases, the slopes recovered completely after irradiation, again for all bias conditions.

Response at High Dose Rate Irradiation

Figure 10 shows the pre- and postirradiation high-dose-rate line regulation characteristics for the "bias without load" case, for a dose of 100 krad(SiO_2).

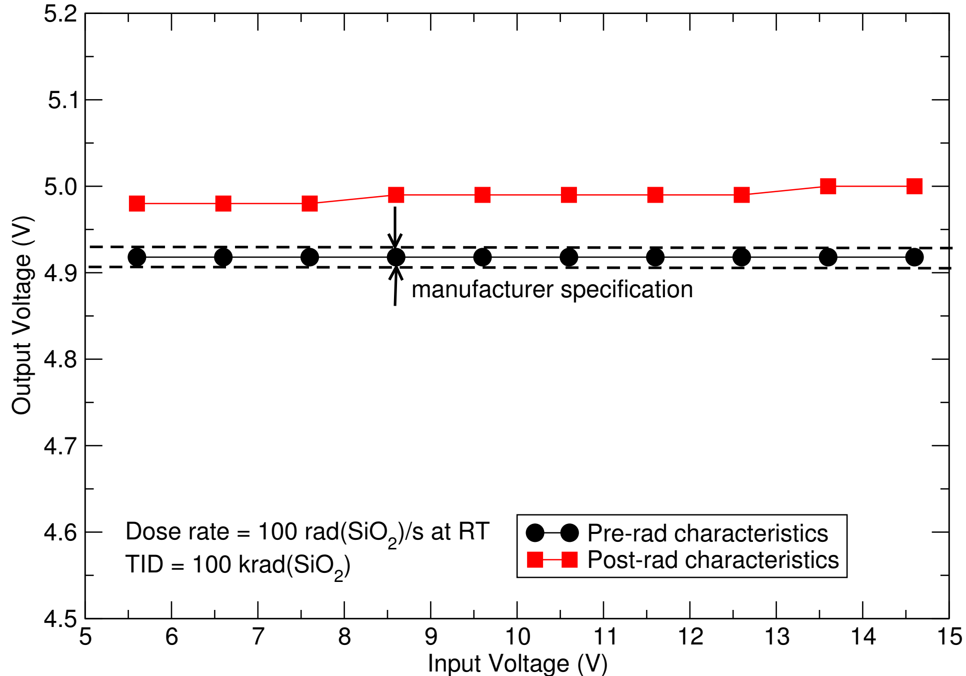

Figure 10: Preirradiation and postirradiation experimental output line regulation characteristics at high dose rate, when the LDO is biased without load during irradiation.

A unique feature observed is that the postirradiation values of V_{out} are greater than corresponding preirradiation values over the entire range of V_{in}. Considering only the postirradiation V_{out} curve, the change in V_{out} over the entire range of V_{in} was within the manufacturer's line regulation specifications [5]. However, when compared to corresponding preirradiation V_{out} values, the change in postirradiation V_{out} exceeds the manufacturer's line regulation specifications [47] significantly.

Figure 11 shows the load regulation response for a dose of 100 krad(SiO_2). Here, V_{out} starts out at a value higher than corresponding preirradiation value and then

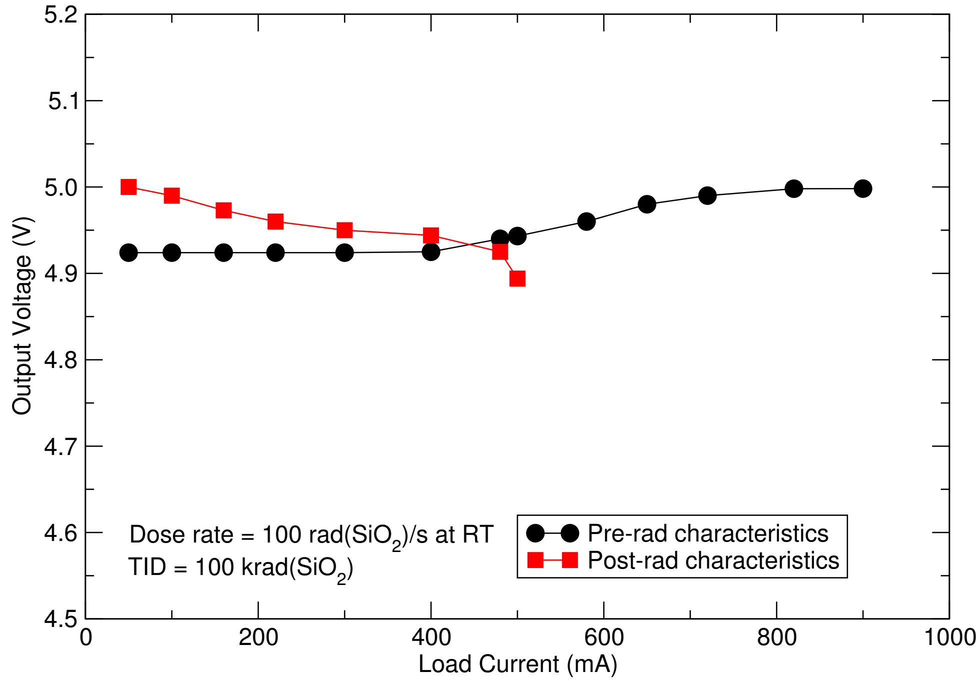

Figure 11: Preirradiation and postirradiation experimental output load regulation characteristics at high dose rate, when the LDO voltage regulator is biased without load during irradiation. Postirradiation output voltages beyond I_{load} of 580 mA are not plotted.

decreases with increasing I_{load} before failing functionally above an I_{load} of 580 mA. Both of the above V_{out} trends in line and load regulation were also observed for the other three bias conditions at high dose rates, irradiated to the same dose, i.e. 100 krad(SiO_2), with the "grounded" bias condition showing the worst response. Of all the parts irradiated at high dose rate to identical doses of 100 krad(SiO_2), those irradiated under "bias with load" conditions exhibited the greatest amount of recovery in line and load regulation during annealing, to within 2% of corresponding preirradiation values. Those parts irradiated under the "grounded" conditions recovered the least during annealing.

CHAPTER VI

ANALYSIS OF THE RADIATION RESPONSE

The responses of the LDO voltage regulator show that the LDR and ETI irradiation conditions produce similar degradation in postirradiation V_{out} (values lower than preirradiation values) for the same dose of 50 krad(SiO_2), with the ETI degradation less than that observed for LDR irradiation. The degradation following HDR irradiation is different from the LDR and ETI results in that the postirradiation V_{out} actually increases above corresponding preirradiation values. This suggests that the circuit-level degradation mechanisms are different for HDR irradiation; this has been confirmed through simulations and experiments on isolated transistors. The results are discussed in detail in the following sections.

Gain Degradation

As seen from Figs. 7, 9, and 11, V_{out} decreased slowly and continually with increasing I_{load} during postirradiation load-regulation characterization for all dose rates and bias conditions. This was caused by gain degradation in the LDO voltage regulator circuit, particularly in the operational amplifier and output pass transistor circuit blocks.

There are two mechanisms in the operational amplifier circuit block of the LDO voltage regulator that account for the shape of the postirradiation output voltage vs. load current plot shown in Fig. 11. After irradiation, the operational amplifier is no longer able to maintain tight feedback because of an increase in its offset

voltage V_{offset} since its bias currents increase. Also, the bias current increases due to increased base-emitter recombination currents in the differential pair transistors, Q_{16} and Q_{17}, which constitute the op amp circuit block. Coupled with the current gain degradation in pass transistor Q_{24}, which is driven by the operational amplifier through the driver transistors, the LDO voltage regulator is no longer able to sustain the supply of higher I_{load}, and V_{out} starts to decrease slowly as I_{load} increases.

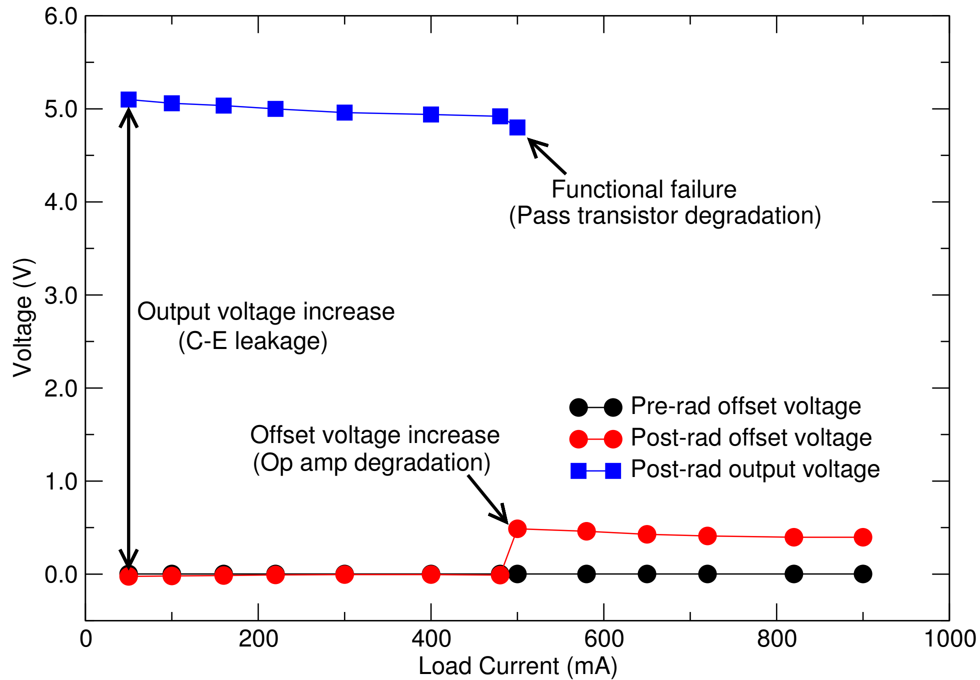

Figure 12: Pre- and post-irradiation offset voltages of the op-amp block show how the droop in the postirradiation output voltage can be modeled as gain degradation in the differential amplifiers and the output pass transistor.

Figure 12 shows the simulation results of the V_{offset} degradation in the operational amplifier circuit block for the high dose rate "bias with load" case. A large increase in V_{offset} is seen around an I_{load} of 500 mA, which is when the LDO voltage regulator functionally fails for irradiation at this bias condition. Simulation results

corresponding to Fig. 12 also show that saturation of the collector current of Q_{24} occurs around the same value of I_{load}. Along with the operational amplifier degradation, this accounts for the functional failure of the LDO voltage regulator.

That the LDO voltage regulator failed completely for LDR irradiation at a dose of 40 krad(SiO_2) in the "grounded" case while it did not in the ETI and HDR cases shows greater gain degradation in the LDR case, which is consistent with the ELDRS effect reported for this LDO voltage regulator in an earlier work [11]. This was also in agreement with the modeling results where the gain for the "grounded" bias condition at LDR was lower than the corresponding value at HDR, while the value at ETI was intermediate.

Collector-Emitter Leakage

The increase in V_{out} during the high dose rate line regulation experiments was caused by degradation in the Brokaw-bandgap circuit, since the internally-generated bandgap-voltage (V_{BG}) influences V_{out} directly, as seen from Eq. (1). Previous work [9] identified collector-emitter (C-E) leakage in the 10× VNPN transistor (Q_1 in this case) of an identical Brokaw-bandgap circuit, observed only at high dose rates (up to 200 krad(SiO_2) in that study) to be the main reason for an increase in V_{out} of another voltage regulator.

In [9], the LM117, a positive voltage regulator was investigated for high and low dose rate responses. The LM117 has an identical Brokaw bandgap circuit [50] as the MIC29372 LDO. Experiments in [9] showed that packaged LM117 test chips with emitter and base of the 10× VNPN transistor shorted and a 30 V reverse bias applied to its base-collector junction showed a C-E leakage similar to one observed

in a "decoupled" 10× VNPN transistor exposed under bias to 200 krad(SiO_2). This was modeled in simulations as a "leakage resistance" connected between the collector and emitter terminals of the above transistor.

The magnitudes of the C-E leakages in the two transistors were different as expected due to differences in the biases applied in the two cases. Also, no C-E leakage was reported for the "decoupled" 10× transistor that was irradiated with all of its leads floating, while no such leakage was observed in any of the cases at low dose rate. In all three cases, an identical high dose rate and total dose of 100 rad(Si)/s and 200 krad(SiO_2) respectively were used. It was suggested that the C-E leakage (observed only at high dose rates) could have been due to the result of a C-E "leakage path" being formed under the large emitter metal area of the 10× transistor under bias during irradiation. This was based on the expectation that the net trapped positive oxide trap charge densities for a given electric field likely are more at high dose rate than at low dose rate due to in-situ annealing that takes place during the latter.

Figure 13 shows how the C-E leakage phenomenon was modeled using a C-E "leakage" resistor between the collector and emitter terminals of Q_1 [9]. The bandgap voltage V_{BG} is the sum of $V_{BE_{(Q2)}}$ and the voltage given by (4), multiplied by a factor corresponding to the voltage division between resistances R_1 and R_2 (V_2), as shown in Fig. 13. Hence, any increase in ΔV_{BE} increases the value of V_{BG}. An increase in the leakage current drives the collector current of Q_1 down, thereby increasing V_{BE} of transistors Q_1 and Q_2, and thus driving up V_{BG}. An increase in V_{BG} correspondingly increases V_{out}. Simulations including a C-E leakage path resistor demonstrated that this mechanism can account for the increase in V_{out} observed experimentally after high dose rate exposure, as shown in Fig. 10.

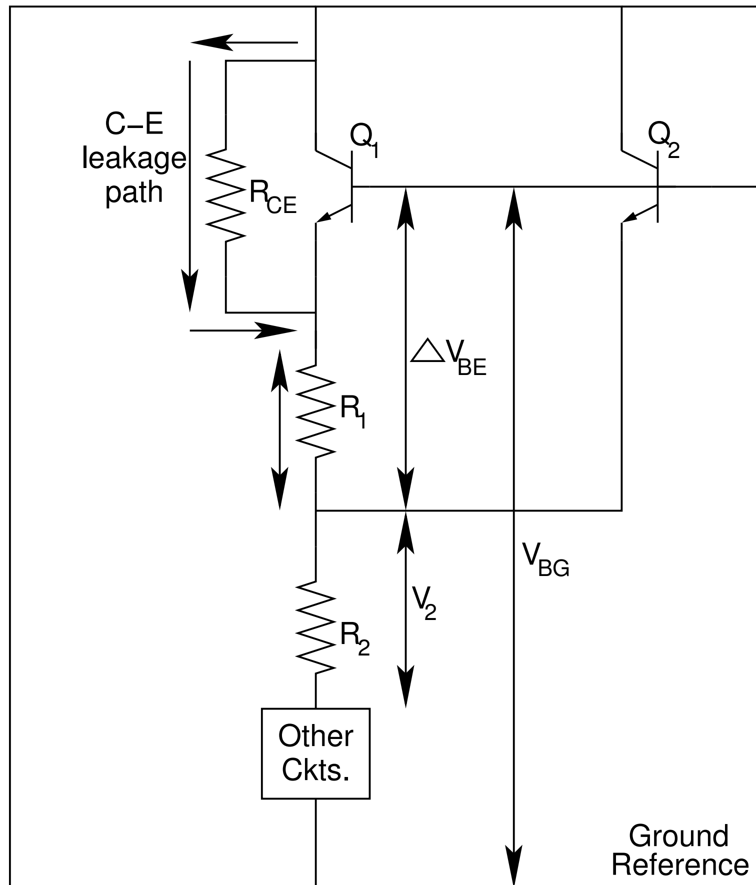

Figure 13: Modeling of C-E leakage by inserting a high-resistance between collector and emitter terminals of Q_1.

The C-E leakage mechanism occurs mainly due to the buildup of radiation-induced positive oxide-trap charge over the base of Q_1. This creates an inversion layer between the collector and emitter. While both Q_1 and Q_2 share a common base with metallization over it, the emitters and collector of Q_1 are placed at some distance from each other, as seen from the die-photo (Fig. 4). This contributes to a greater C-E leakage in the $10\times$ Q_1 than in the $1\times$ Q_2. When bias is applied to the LDO voltage regulator, it induces a larger positive electric field in the p-base in Q_1 as compared to the case when all of the LDO pins are grounded during irradiation, leading to the

formation of more oxide-trap charge in the case when Q_1 is biased. Hence, V_{out} has a higher value postirradiation in the case where the LDO was biased during irradiation as compared to corresponding values in the case when all of its pins were grounded during irradiation. More description of the dependence of V_{out} changes for different irradiation biases is given in [14]. The starting value of V_{out} in the postirradiation load regulation plot of Fig. 11 is also higher than its corresponding preirradiation value due to the C-E leakage.

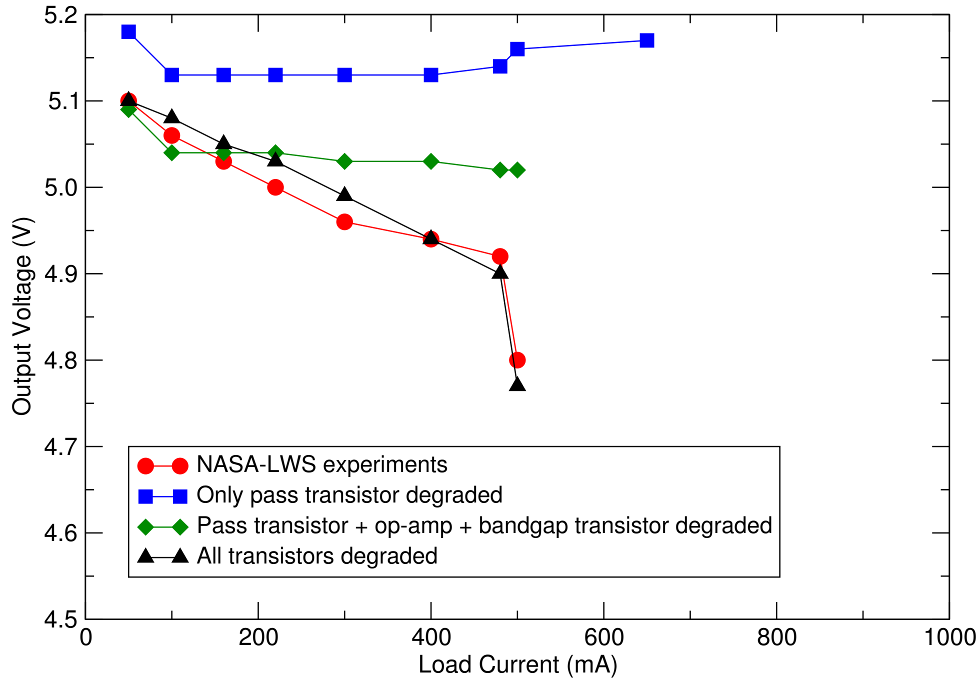

Figure 14: Simulation results showing the influence of pass transistor degradation on the load regulation response of the LDO in the case where the LDO is biased and loaded during irradiation. Output voltages that go below 4.5 V for higher load currents are not plotted.

Figure 14 shows the simulation results of modeling the C-E leakage phenomenon for load regulation for the case in which the LDO voltage regulator was biased and loaded during irradiation. It can be clearly seen that the output pass transistor

bounds the load regulation response to a large extent since it conducts most of the load current. The effect of the op amp degradation scales the load regulation curve downwards while the contribution of other transistors in the circuit to the load regulation degradation is minimal in comparison.

The existence of the C-E leakage phenomenon was verified by direct measurement of the pre- and postirradiation Gummel curves of the transistor in question, i.e. Q_1. Bare MIC29372 die were procured from a Micrel vendor. Transistor Q_1 was isolated from the rest of the LDO voltage regulator circuit using a focused ion beam (FIB). Gummel curves were obtained by micro-probing the isolated Q_1 and using a HP 4156 parametric analyzer. The base-emitter voltage V_{BE} was swept from 0 V to 0.8 V, while maintaining the collector-emitter voltage V_{CE} at 2 V. This procedure was carried out successfully for three die samples, with similar results obtained in each case.

A fresh MIC29372 LDO die was biased through its input pads to +15 V using a micro-probe, and then irradiated at this bias with a 10 keV X-ray source at Vanderbilt University. No load was connected at the output of the die, corresponding to the "bias with no load" case in the experiments. The dose rate and total doses were 100 rad(SiO_2)/s and 200 krad(SiO_2), respectively. Transistor Q_1 was then isolated and characterized.

Figure 15 illustrates the pre- and post-irradiation results. The postirradiation collector current of Q_1 shows a leakage current of about 1 μA at lower values of V_{BE}, clearly showing the effect of C-E leakage. This leakage current does not exist when

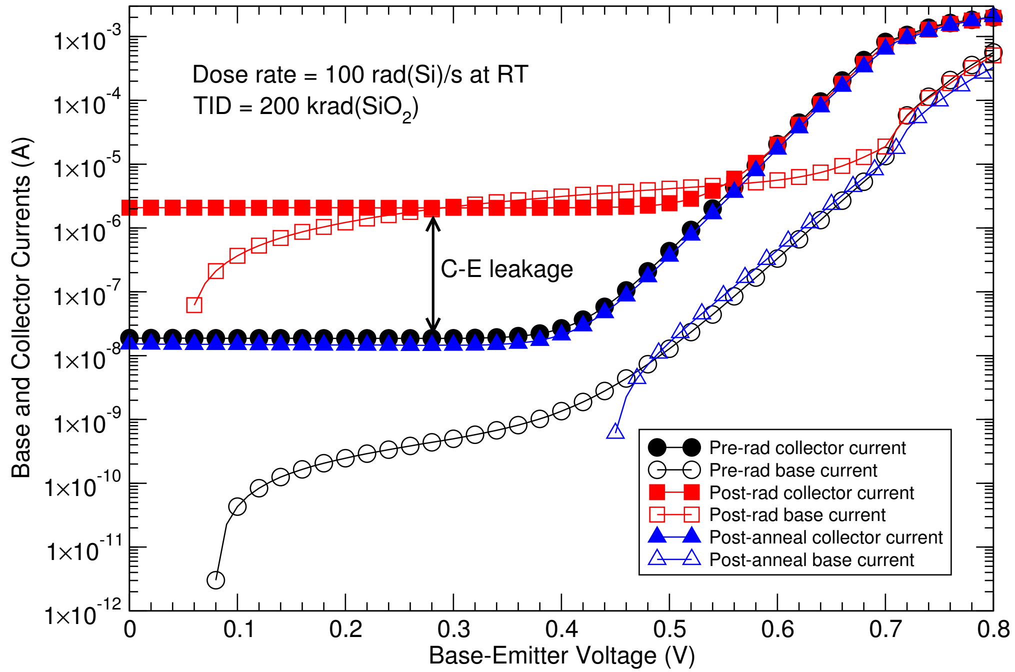

Figure 15: Pre- and post-irradiation and post-anneal characterization of the 10× bandgap transistor Q_1.

the parts are irradiated at lower dose rates or at elevated temperature because of in-situ annealing. The post-irradiation anneal of the C-E leakage is due to the annealing of oxide-trap charge, as discussed further in the next chapter.

The postirradiation anneal of base current I_b at RT to close to corresponding preirradiation values might suggest that the base of Q_1 probably goes back to accumulation once the oxide-trap charges have annealed. This would "decrease" its value due to lack of carriers and thus shift the post-anneal I_b curve downwards.

Summary of Modeling Parametric Variations

Figures 16 through 18 summarize the modeling of three key transistor parameters in terms of normalized changes of their values pre- and postirradiation for all dose rates and bias conditions. These parameters were chosen since their "degradation"

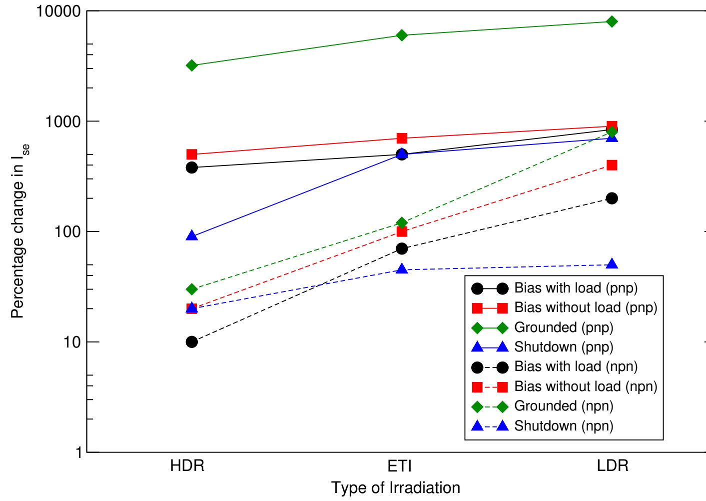

Figure 16: Modeled changes in I_{se} for all three dose rates and corresponding bias conditions. The dashed lines represent modeling for NPNs while the solid lines represent the modeling done for PNPs.

due to irradiation was most likely to affect the operation of the transistors in the LDO circuit. The key parameters were the forward DC gain β_F, the base-emitter recombination current I_{se}, and the ideality factor N_e. The values of the electrical parameters were chosen to emulate the actual response seen in the NASA-LWS experiments for the three types of radiation dose-rates considered.

It can be seen in Figs. 16 through 18 that PNP transistors (including the LPNP output pass transistor and the diff-amps) were "degraded" more than NPNs in the LDO circuit to emulate the experimental data. This is consistent with previous work [48, 49] that shows that PNP transistors typically degrade more than NPN devices. Also, the degradation was greater at LDR than the corresponding degradation at HDR and ETI in most of the cases, as reported in previous work [10, 11] and also observed in the NASA-LWS experiments.

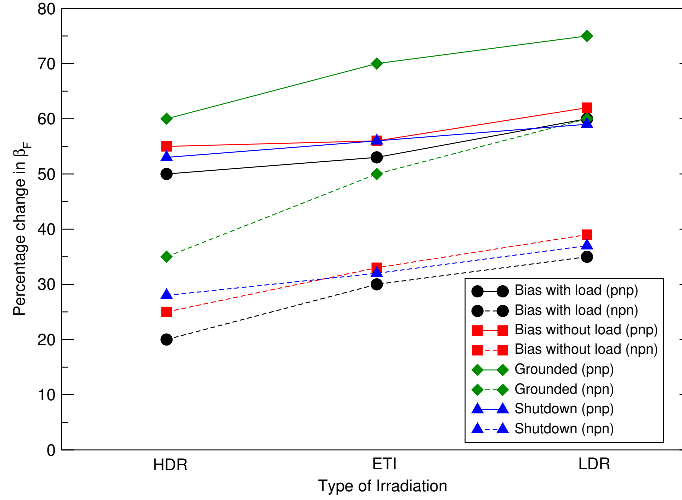

Figure 17: Modeled changes in β_F for all three dose rates and corresponding bias conditions. The dashed lines represent modeling for NPNs while the solid lines represent the modeling done for PNPs.

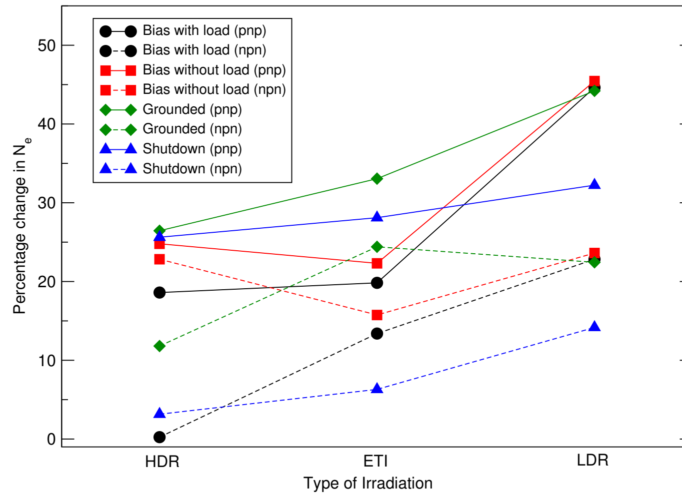

Figure 18: Modeled changes in N_e for all three dose rates and corresponding bias conditions. The dashed lines represent modeling for NPNs while the solid lines represent the modeling done for PNPs.

CHAPTER VII

ANNEALING MECHANISMS

Annealing after High Dose Rate Irradiation

High dose rate line and load regulation characteristics were measured after 16 and 74 days of room-temperature annealing. Considering the two extreme cases, the "bias with load" device had a die temperature of 100°C because of the I_{load} flowing at the output, while the "grounded" device remained at RT during anneal. Figure 19 shows that the former bias condition had a near-complete recovery in load regulation toward corresponding preirradiation V_{out} characteristics after both anneals [14].

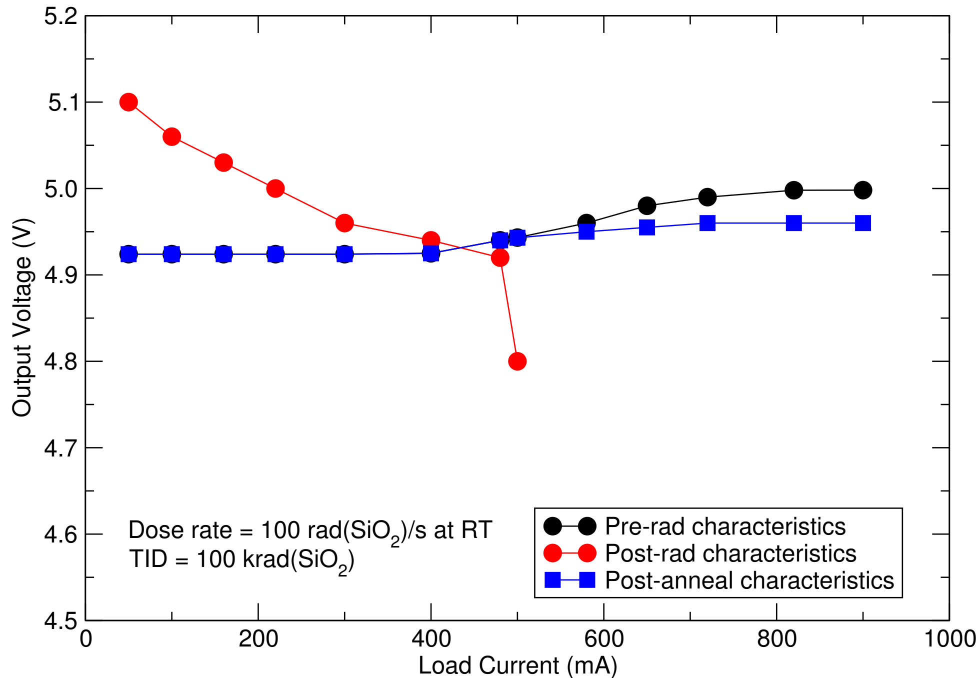

Figure 19: Experimental postirradiation anneal for high dose rate, bias with load, load regulation characteristics. The second anneal curve is not plotted since it overlaps the first one.

At higher $I_{load,}$ the post-anneal load regulation V_{out} does not recover to its corresponding preirradiation values, while it does so completely at lower values of I_{load}, which is consistent with annealing of oxide-trap charge during either lower-rate irradiation (in-situ annealing) or postirradiation annealing [48]. A significant annealing effect was also seen in the isolated-Q_1 experiment, as shown in Fig. 15, where the postirradiation C-E leakage went down to near the preirradiation values after RT annealing. This is also consistent with enhanced annealing of oxide-trap charge for the loaded devices irradiated at higher dose rates, owing to the accelerated rate at which oxide-trap charge anneals or is neutralized by compensating electron trapping at elevated temperature [49].

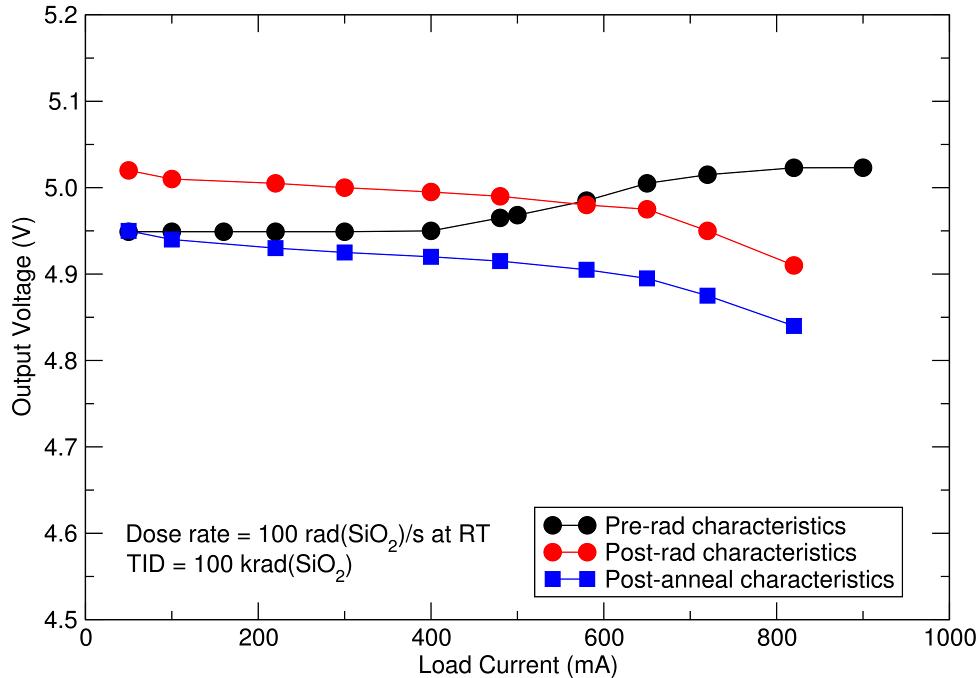

Figure 20: Experimental postirradiation anneal for high dose rate, grounded load regulation characteristics. The second anneal curve is not plotted since it overlaps the first one.

In line regulation, there was near-complete recovery towards corresponding preirradiation V_{out} characteristics after both anneals [14]. In contrast, Fig. 20 shows that, for the "grounded" case, the load regulation slope does not show recovery — this likely is because there is less annealing of oxide trap charge, since the die never experienced high temperatures (either due to I_{load} or external environment) during anneal.

In addition, there was no recovery in either the slope or magnitude of V_{out} towards corresponding preirradiation values after both anneals, in line regulation [14]. A probable cause for the parallel downward shift of the load regulation curve could be un-annealed interface traps that remain after all of the oxide-trap charges anneal out.

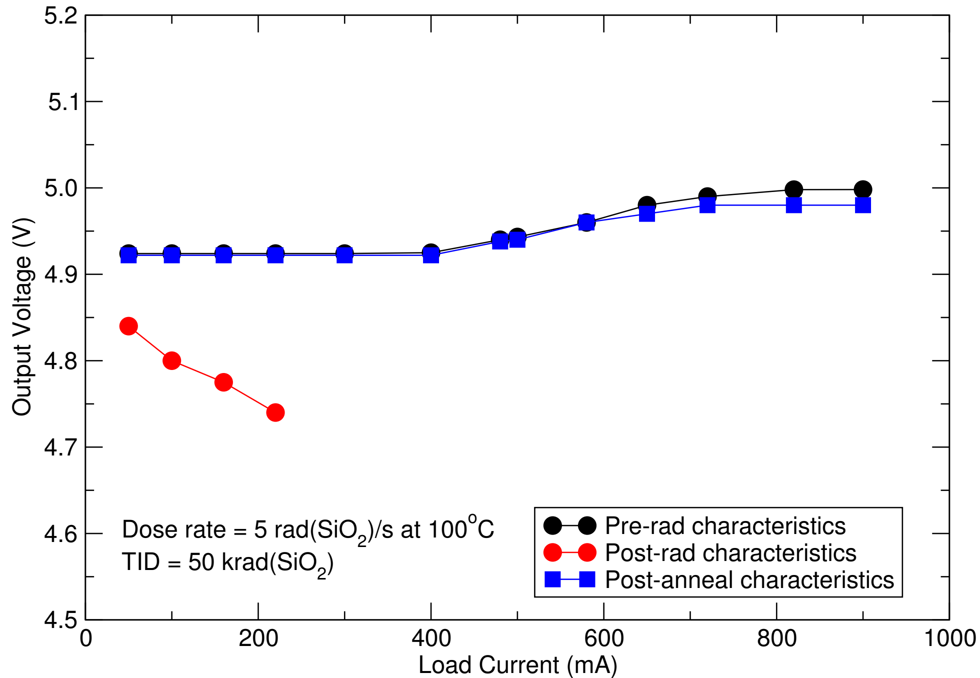

Figure 21: Experimental postirradiation anneal for elevated temperature irradiation, bias without load, load regulation characteristics. The second anneal curve is not plotted since it overlaps the first one.

Annealing after Elevated Temperature Irradiation

In the ETI line and load regulation experiments, annealing was done at 100°C. Again, annealing measurements were carried out after 14 and 35 days. There was no "load" current flowing at the output, since the die temperature was already at 100°C. Figure 21 shows how all measured parameters recover significantly [14].

There was complete recovery of both slope and magnitude, even in line regulation [14]. Both the line and load regulation results are consistent with the annealing of interface traps at 100°C. Earlier studies [51]-[53] have found similar results at low electric fields at similar temperatures, suggesting that interface-trap annealing is responsible for the observed recovery.

CHAPTER VIII

CONCLUSIONS

Simulations and experimental results show that collector-emitter leakage of a critical NPN transistor in the Brokaw band-gap circuit, associated with enhanced oxide-trap charge during high dose rate exposures, is responsible for some of the most significant changes in circuit response for the MIC29372 LDO voltage regulator under various bias conditions at a high dose rate. The collector-emitter leakage phenomenon is thus the limiting factor in determining the circuit response at high dose rates. For lower dose rates, a steady decrease in output voltage with increasing load current is observed. Modeling this decrease as gain degradation in the differential pair transistors forming the operational amplifier circuit block and that of the output pass transistor emulates the total ionizing dose functional failures observed in the LDO voltage regulator. The circuit response at low dose rates is thus limited by gain degradation in the LDO circuit.

A near-complete recovery of output and regulation characteristics at lower load currents is observed after annealing after high dose-rate and elevated temperature irradiation. This recovery is associated with the annealing of interface traps at elevated temperatures associated either with the ambient temperature during annealing, or with the power dissipation associated with loaded circuit operation. The behavior of this LDO voltage regulator contrasts with earlier studies that have shown that operational amplifiers and comparators become worse after annealing due to increased

postirradiation interface trap formation. The development of calibrated circuit models greatly facilitates the understanding of the LDO voltage regulator response over a wide range of experimental conditions. These models should enable further insight into the responses of these and similar devices in the space radiation environment.

REFERENCES

[1] Joel N. Shurkin, "Broken Genius: The Rise and Fall of William Shockley: Creator of the Electronic Age," *New York: MacMillan*, 2006.

[2] G. C. Messenger and J. P. Spratt, "The Effects of Neutron Irradiation on Germanium and Silicon," *Proc. IRE*, vol. 46, pp. 1038-1044, 1958.

[3] T. P. Ma and P. V. Dressendorfer, Eds., "Ionizing Radiation Effects in MOS Devices and Circuits," *New York: Wiley*, 1989.

[4] D. S. Peck and R. R. Blair. W. L. Brown and F. M. Smits, "Surface Effects of Radiation Transistors," *Bell System Technical Journal*, vol. 42, pp. 95-129, 1963.

[5] R. L. Pease, "Total Ionizing Dose Effects in Bipolar Devices and Circuits," *IEEE Trans. Nucl. Sci.*, vol. 50, No. 3, pp. 539-551, 2003.

[6] S. Subbanna, J. Johnson, G. Freeman, R. Volant, R. Groves, D. Herman, and B. Meyerson, "Prospects of Silicon-Germanium-based Technology for Very High-Speed Circuits," *IEEE Microwave Symposium Digest*, pp. 361-364, 2000.

[7] R. M. Warner Jr., and R. D. Schrimpf, "BJT-MOSFET Transconductance Comparisons," *IEEE Trans. Electron Devices*, vol. ED-34, pp. 1061-1065, 1987.

[8] J. T. Beacour, T. Carriere, A. Gach, D. Laxague and P. Poirot, "Total Dose Effects on Negative Voltage Regulator," *IEEE Trans. Nucl. Sci.*, vol. 41, No. 6, pp. 2420-2426, December 1994.

[9] H. J. Barnaby, H. J. Tausch, R. Turfler, P. Cole, P. Baker, and R. L. Pease, "Analysis of Bipolar Linear Circuit Response Mechanisms for High and Low Dose Rate Total Dose Irradiations," *IEEE Trans. Nucl. Sci.*, vol. 43, No. 6, pp. 3040-3048, December 1996.

[10] R. L. Pease, W. E. Combs, A. Johnston, T. Carriere, C. Poivey, A. Gach, and S. McClure, "A Compendium of Recent Total Dose Data on Bipolar Linear Microcircuits," *IEEE Radiation Effects Data Workshop Record*, pp. 28-37, 1996.

[11] R. L. Pease, S. McClure, A. H. Johnston, J. Gorelick, T. L. Turflinger, M. Gehlhausen, J. Krieg, T. Carriere, and M. Shaneyfelt, "An Updated Compendium of Enhanced Low Dose Rate Sensitive (ELDRS) Bipolar Linear Circuits," *IEEE Radiation Effects Data Workshop Record*, pp. 127-133, 2001.

[12] S. S. McClure, R. L. Pease, W. Will and G. Perry, "Dependence of Total Dose Response of Bipolar Linear Microcircuits on Applied Dose Rate," *IEEE Trans. Nucl. Sci.*, vol. 41, No. 6, pp. 2544-2549, December 1994.

[13] S. S. McClure, A. H. Johnston, J. L. Gorelick and R. L. Pease, "Total Dose Performance of Radiation-Hardened Voltage Regulators and References," *IEEE Radiation Effects Data Workshop*, pp. 1-5, 2001.

[14] R. L .Pease, G. Dunham, and J. Seiler, "Total Dose and Dose-Rate Response of Low-Dropout Voltage Regulators," presented at the *IEEE Radiation Effects Data Workshop, 2006*.

[15] G. C. Messenger and R. A. Hubbs, "A General Proof of the Beta Degradation Equation for Bulk Displacement Damage," *IEEE Trans. Nucl. Sci.*, vol. 20, 1973.

[16] G. C. Messenger and M. S. Ash, "The Effects of Radiation on Electronic Systems," *New York: Van-Nostrand-Reinhold* , 1986.

[17] C. J. Dale, P. W. Marshall, E. A. Burke, G. P. Summers, and E. A. Wolicki, "High Energy Electron Induced Displacement Damage in Silicon," *IEEE Trans. Nucl. Sci.*, vol. 35, pp. 1208-1214, December 1988.

[18] S. L. Kosier, R. D. Schrimpf, A. Wei, M. DeLaus, D. M. Fleetwood, and W. E. Combs, "Effects of Oxide Charge and Surface Recombination Velocity on the Excess Base Current of BJTs," *Proc. IEEE Bipolar/BiCMOS Circuits and Technology Meeting*, pp. 211-214, 1993.

[19] R. N. Nowlin, R. D. Schrimpf, E. W. Enlow, W. E. Combs and R. L. Pease, "Mechanisms of Ionizing-Radiation-Induced Gain Degradation in Modern Bipolar Devices," *Proc. IEEE Bipolar Circuits and Tech. Mtg.*, pp. 174.177, 1991.

[20] S. L. Kosier, A. Wei, R. D. Schrimpf, D. M. Fleetwood, M. DeLaus, R. L. Pease, and W. E. Combs, "Physically Based Comparison of Hot-Carrier-Induced and Ionizing-Radiation-Induced Degradation in BJTs," *IEEE Trans. Electron Devices*, vol. 42, pp. 436-444, 1995.

[21] D. M. Schmidt, A. Wu, R. D. Schrimpf, D. M. Fleetwood, and R. L. Pease, "Modeling Ionizing-Radiation-Induced Gain Degradation of the Lateral PNP Bipolar Junction Transistor," *IEEE Trans. Nucl. Sci.*, vol. 43, pp. 3032-3039, December 1996.

[22] H. J. Barnaby, R. J. Milanowski, R. D. Schrimpf, L. W. Massengill, and M. Pagey, "Modeling Ionizing Radiation Effects in Lateral PNP BJTs with Non-Uniform Trapped Charge Distributions," *GOMAC Dig.*, pp. 585-588, 1998.

[23] H. J. Barnaby, R. D. Schrimpf, D. M. Fleetwood, and S. L. Kosier, "The Effects of Emitter-Tied Field Plates on Lateral PNP Ionizing Radiation Response," *IEEE BCTM Proc.*, pp. 35-38, 1998.

[24] H. J. Barnaby, C. Cirba, R. D. Schrimpf, S. L. Kosier, P. Fouillat, and X. Montagner, "Modeling BJT Radiation Response with Non-Uniform Energy Distributions of Interface Traps," *IEEE Trans. Nucl. Sci.*, vol. 47, pp. 514-518, December 2000.

[25] H. J. Barnaby, R. D. Schrimpf, and R. L. Pease, "Influence of Interface and Bulk Defect Interaction on Proton Radiation Response of Bipolar Devices," *IEEE Trans. Nucl. Sci.*, vol. 48, No. 6, pp. 2074-2080, December 2001.

[26] B. G. Rax, A. H. Johnston, and T. Miyahira, "Displacement Damage in Bipolar Linear Integrated Circuits," *IEEE Trans. Nucl. Sci.*, vol. 46, pp. 1660-1665, December 1999.

[27] J. A. Zoutendyk, C. A. Goben, and D. F. Berndt, "Comparison of the Degradation Effects of Heavy Ion, Electron, and Cobalt-60 Irradiation in an Advanced Bipolar Process," *IEEE Trans. Nucl. Sci.*, vol. 35, pp. 1428-1431, December 1988.

[28] E. W. Enlow, R. L. Pease, W. E. Combs, R. D. Schrimpf and R. N. Nowlin, "Response of Advanced Bipolar Processes to Ionizing Radiation," *IEEE Trans. Nucl. Sci.*, vol. 38, pp. 1342-1351, December 1991.

[29] R. D. Schrimpf, "Physics and Hardness Assurance for Bipolar Technologies," *IEEE NSREC Short Course*, pp. 202-269, 2001.

[30] A. H. Johnston, G. M. Swift and B.G. Rax, "Total Dose Effects in Conventional Bipolar Transistors and Linear Integrated Circuits," *IEEE Trans. Nucl. Sci.*, vol. 41, pp. 2427-2436, December 1994.

[31] D. M. Fleetwood, S. L. Kosier, R. N. Nowlin, R. D. Schrimpf, R. A. Reber, Jr., M. DeLaus, P. S. Winokur, A. Wei, W. E. Combs, and R. L. Pease, "Physical Mechanisms Contributing to Enhanced Bipolar Gain Degradation at Low Dose Rates," *IEEE Trans. Nucl. Sci.*, vol. 41, pp. 1871-1883, December 1994.

[32] R. J. Graves, C. R. Cirba, R. D. Schrimpf, R. J. Milanowski, A. Michez, D. M. Fleetwood, S. C. Witczak, and F. Saigne, "Modeling Low-Dose-Rate Effects in Irradiated Bipolar-Base Oxides," *IEEE Trans. Nucl. Sci.*, vol. 45, pp. 2352-2360, 1998.

[33] S. N. Rashkeev, C. R. Cirba, D. M. Fleetwood, R. D. Schrimpf, S. C. Witczak, A. Michez, and S. T. Pantelides, "Physical Model for Enhanced Interface-Trap Formation at Low Dose Rates," *IEEE Trans. Nucl. Sci.*, vol. 49, pp. 2650-2655, 2002.

[34] D. M. Fleetwood, L. C. Riewe, J. R. Schwank, S. C. Witczak, and R. D. Schrimpf, "Radiation Effects at Low Electric Fields in Thermal, SIMOX, and Bipolar-Base Oxides," *IEEE Trans. Nucl. Sci.*, vol. 43, pp. 2537-2546, December 1996.

[35] S. C. Witczak, R. C. Lacoe, D. C. Mayer, D. M. Fleetwood, R. D. Schrimpf, and K. F. Galloway, "Space Charge Limited Degradation of Bipolar Oxides at Low Electric Fields," *IEEE Trans. Nucl. Sci.*, vol. 45, pp. 2339-2351, December 1998.

[36] R. K. Freitag and D. B. Brown, "Low Dose Rate Effects on Linear Bipolar IC's: Experiments on the Time Dependence," *IEEE Trans. Nucl. Sci.*, vol. 44, pp. 1906-1913, December 1997.

[37] R. K. Freitag and D. B. Brown, "Study of Low-Dose-Rate Radiation Effects on Commercial Linear Bipolar ICs," *IEEE Trans. Nucl. Sci.*, vol. 45, pp. 2649-2658, December 1998.

[38] V. V. Belyakov, V. S. Pershenkov, A. V. Shalnov, and I. N. Shvetzov-Shilovsky, "Use of MOS Structure for Investigation of Low-Dose-Rate Effect in Bipolar Transistors," *IEEE Trans. Nucl. Sci.*, vol. 42, pp. 1660-1666, December 1995.

[39] J. Boch, F. Saigne, A. D. Touboul, S. Ducret, J. F. Carlotti, M. Bernard, R. D. Schrimpf, F. Wrobel, and G. Sarrabayrouse, "Dose Rate Effects in Bipolar Oxides: Competition between Trap Filling and Recombination," *Applied Physics Letters*, vol. 88, pp. 232113, 2006.

[40] R. L. Pease, R. M. Turfler, D. Platteter, D. Emily, and R. Blice, "Total Dose Effects in Recessed Oxide Digital Bipolar Microcircuits," *IEEE Trans. Nucl. Sci.*, vol. NS-30, pp. 4216-4223, December 1983.

[41] J. L. Titus and D. G. Platteter, "Wafer Mapping of Total Dose Failure Thresholds in a Bipolar Recessed Field Oxide Technology," *IEEE Trans. Nucl. Sci.*, vol. 34, pp. 1751- 1756, December 1987.

[42] E. W. Enlow, R. L. Pease, W. E. Combs, and D. G. Platteter, "Total Dose Induced Hole Trapping in Trench Oxides," *IEEE Trans. Nucl. Sci.*, vol. 36, pp. 2415-2422, December 1989.

[43] J. P. Raymond, R. A. Gardner, and G. E. LaMar, "Characterization of Radiation Effects on Trench-Isolated Bipolar Analog Microcircuit Technology," *IEEE Trans. Nucl. Sci.*, vol. 39, pp. 405-412, December 1992.

[44] W. C. Jenkins, "Dose-Rate-Independent Total Dose Failure in 54F10 Bipolar Logic Circuits," *IEEE Trans. Nucl. Sci.*, vol. 39, pp. 1899-1902, December 1992.

[45] V. Ramachandran, B. Narasimham, D. M. Fleetwood, R. D. Schrimpf, W. T. Holman, A. F. Witulski, G. Dunham, J. Seiler and D. Platteter, "Modeling Total-Dose Effects for a Low-Dropout Voltage Regulator," in publication, in *IEEE Trans. Nucl. Sci.*, vol. 53, No. 6, December 2006.

[46] NASA website, http://lws.gsfc.nasa.gov/documents/mowg_june2003/set_report.pdf.

[47] MIC29372 datasheet, Micrel Inc, May 2006.

[48] R. D. Schrimpf, R. J. Graves, D. M. Schmidt, D. M. Fleetwood, R. L. Pease, W. E. Combs, and M. DeLaus, "Hardness Assurance Issues for Lateral PNP Bipolar Junction Transistors," *IEEE Trans. Nucl. Sci.*, vol. 42, No. 6, pp. 1641-1649, 1995.

[49] D. M. Fleetwood, S. L. Miller, R. A. Reber, Jr., P. J. McWhorter, P. S. Winokur, M. R. Shaneyfelt, and J. R. Schwank, "New Insights Into Radiation-Induced Oxide-Trap Charge Through Thermally-Stimulated-Current Measurement and Analysis," *IEEE Trans. Nucl. Sci.*, vol. 39, No. 6, pp. 2192-2203, 1992.

[50] LM117 datasheet, National Semiconductor, June 2006.

[51] R. L. Pease, D. G. Platteter, G. W. Dunham, J. E. Seiler, H. J. Barnaby, R.D. Schrimpf, M. R. Shaneyfelt, M. C. Maher, and R. N. Nowlin, "Characterization of Enhanced Low Dose Rate Sensitivity (ELDRS) Effects Using Gated Lateral PNP Transistor Structures," *IEEE Trans. Nucl. Sci.*, vol. 51, No.6, pp. 3773-3780, 2004.

[52] M. R. Shaneyfelt, J. R. Schwank, D. M. Fleetwood, R. L. Pease, J. A. Felix, P. E. Dodd, and M. C. Maher, "Annealing Behavior of Bipolar Linear Devices with Enhanced Low-Dose-Rate Sensitivity," *IEEE Trans. Nucl. Sci.*, vol. 51, No. 6, pp. 3172-3177, 2004.

[53] D. M. Fleetwood, P. V. Dressendorfer, and D. C. Turpin, "A Reevaluation of Worst-Case Postirradiation Response for Hardened MOS Transistors," *IEEE Trans. Nucl. Sci.*, vol. 34, No. 6, pp. 1178-1183, 1987.